



Review

Methods for Evaluating Friction between Intravascular Device and Vascular Biomodel

Kazuto Takashima ^{1)*}, Makoto Ohta²⁾, Kiyoshi Yoshinaka³⁾, Toshikatsu Washio³⁾ and Kiyoyuki Chinzei³⁾

¹⁾Graduate School of Life Science and Systems Engineering, Kyushu Institute of Technology,
2-4 Hibikino, Wakamatsu-ku, Kitakyushu, Fukuoka 808-0196, Japan

²⁾Institute of Fluid Science, Tohoku University,
2-1-1 Katahira, Aoba-ku, Sendai, Miyagi 980-8577, Japan

³⁾Health and Medical Research Institute, National Institute of Advanced Industrial Science and Technology,
1-2-1 Namiki, Tsukuba, Ibaraki 305-8564, Japan

*Corresponding author: Kazuto Takashima (ktakashima@life.kyutech.ac.jp)

Manuscript received 31 October 2023; accepted 04 February 2024; published 29 February 2024

Abstract

In recent years, endovascular treatments, in which a treatment device such as a catheter is inserted into a blood vessel to directly approach a lesion, have become increasingly popular worldwide. For safer treatment and further optimization of medical devices, a deeper understanding of the vascular biotribology of the medical devices, biomodels, and blood vessels and an appropriate evaluation method are required. This review paper presents the current state of research on the evaluation of the friction between an intravascular device and a vascular biomodel. We review the experimental conditions, including the sample shape, sliding speed, contact pressure, lubricant, materials, and temperature. Standardized methods should be established for evaluating the friction between an intravascular device and a vascular biomodel.

Keywords

endovascular treatment, biotribology, catheter, guidewire, blood vessel, friction, biomodel

1 Introduction

Intravascular medical devices such as catheters, guidewires, stents, and coils are used for the treatment of various diseases, including infarction and aneurysms (Fig. 1). In such endovascular treatments, medical devices are inserted into blood vessels with guidance provided by X-ray angiography, where a contrast agent is injected to allow X-ray imaging of the blood vessels. During a catheterization procedure in blood vessels, the surgeon directs a guidewire through the patient's arterial system to the desired position by inserting, retracting, and turning the guidewire at the point of insertion (upper part of Fig. 1). A catheter is then slipped over the guidewire until it reaches the desired location, where it is used to perform various procedures (e.g., coil embolization, balloon angioplasty, and stent insertion, lower part of Fig. 1). In recent years, endovascular treatments have become increasingly popular worldwide because they allow lesions to be approached without the need for wide tissue incisions. However, these treatments are sometimes difficult because the blood vessel caliber is small and vessels have many twists and turns. For example, the inner diameter of the distal part of an internal carotid artery is about 4 mm [1, 2]. Many cerebral aneurysms form at the internal carotid

artery, which has a highly curved part called the carotid siphon [3]. The curvature of many parts of the carotid artery is less than 0.5 1/mm [3, 4]. Furthermore, the surgeon's sensory perception (visual and tactile) is severely reduced during manipulation in such treatments because many intravascular medical devices are long and flexible with few degrees of freedom (e.g., pushing, pulling, and twisting at the proximal portion from outside the human body, upper part of Fig. 1). Moreover, the frictional force applied by the medical device on the blood vessel wall can induce vasoconstriction, injury, and perforation and can result in reactive intimal proliferation or distal embolization associated with end-organ ischemia and infarction [5–7]. In the case of cardiovascular catheters, damage to blood vessels near the heart can cause hemorrhagic shock, which is a life-threatening condition [8].

Furthermore, the precise delivery of a medical device is prevented by unpredictable changes in friction. Specifically, the changing contact and friction between the medical device and a blood vessel make the mechanics complicated. Consequently, friction diminishes the effectiveness or sometimes even prevents the successful use of the device, necessitating the use of more risky, complicated, and costly procedures. For example, inappropriate techniques can increase the number of trial-and-

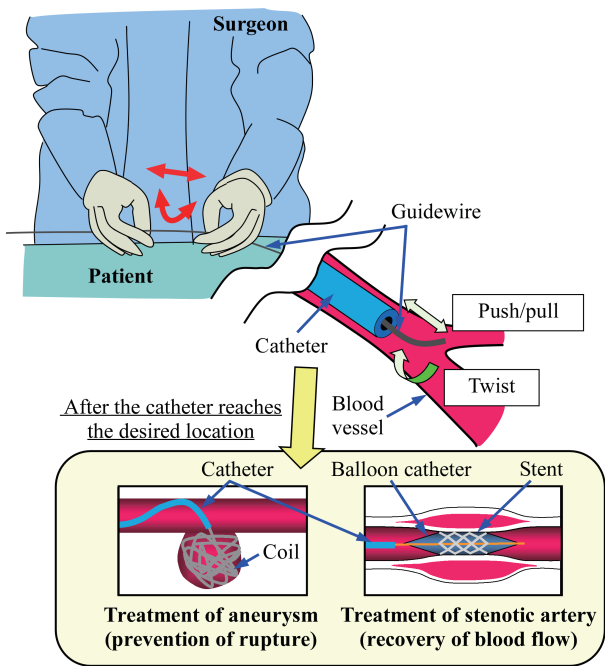


Fig. 1 Schematic diagram of endovascular treatment using catheter, guidewire, stent, and coil

error attempts during treatment, which can cause vascular endothelial damage and prolonged exposure to radiation for both patients and neurosurgeons [9].

Scaffold-like stents, such as coronary artery or carotid artery stents, are used to stabilize the vessel diameter and blood flow (lower right panel of Fig. 1). Similar stent grafts are used for the endovascular repair of an abdominal aortic aneurysm. The friction between the device materials and endothelial cells affects the migration and displacement of the stent [10] and the stent graft [11, 12] after deployment. Moreover, the shearing force applied on a balloon-expandable vascular stent mounted on a delivery system could displace and dislodge the stent during the delivery process [13]. Furthermore, in vascular anastomosis, the friction between the device and the vessel wall significantly affects the success of procedures [14, 15].

Therefore, many studies have attempted to reduce the friction between the medical device and the vessel. For example, a hydrophilic polymer surface has been developed to provide lubricity to catheters [7, 8, 16–23]. However, high catheter lubricity sometimes results in the application of excessive force to the catheter tip, leading to perforation of the blood vessel [24]. Therefore, a simple and reliable method for quantifying the subjective feeling of slipperiness and lubricity between the medical device and the vessel is required. In order to realize atraumatic advancement and precise positioning while avoiding local obstacles, device performance must be characterized based on the mechanical properties of the device, which should be measured using standard methods under reproducible conditions.

Biomodels that mimic various types of vasculature [9, 25–40] can be used to test new endovascular medical devices and teach techniques to medical personnel; they also allow the practice and planning of procedures before treatment without exposing patients to X-rays. Moreover, biomodels are more economical and ethical compared to human cadavers and animals. Furthermore, it is very difficult to keep the

experimental conditions constant for animal blood vessels [7]. In order to provide an accurate simulation environment, biomodels should be as similar as possible to actual blood vessels. Because medical devices make contact with biomodels, the mechanical properties of biomodels, such as their friction, viscoelasticity, and surface shape, have a large effect on the behavior of medical devices. Therefore, vascular models must have flexibility (elastic modulus) similar to that of vascular tissue and appropriate sliding (surface friction) that mimics the vascular lumen [41]. However, as there are no standard methods for evaluating these properties, the mechanical properties differ among medical models.

Numerical analysis models [12, 26, 27, 42–55] have been developed for medical education, surgical training, surgical planning, intra-operative assistance, and medical device design. These models require tissue models with realistic responses. For example, in practice, an instrument encounters friction, which changes its path through the vascular system [42, 55]. Accurate friction parameters are thus required. Experimental data can be used for the validation of new methods for predicting the contact force between a catheter and a vascular artery [56].

Accurate frictional properties of the biomodel and medical devices are expected to improve interventional neuroradiology robotic systems [57–63]. Furthermore, friction affects the magnetic navigation of an untethered device in an artery [64, 65].

As described above, various experimental methods can be used to measure the frictional force between medical devices and vessel walls or biomodels. However, there is no established quantitative rating system for objectively evaluating and validating these devices. Therefore, in this review, we present the current state of research on the evaluation of the interaction between intravascular devices and blood vessels or vascular models. The properties measured under strictly controlled and well-defined conditions provide a framework for systematic comparisons between devices, facilitating the development of more efficient intravascular devices [66]. Moreover, an objective evaluation method will help end users differentiate between devices and understand the strengths and weaknesses of each device.

The rest of this article is organized as follows. In Section 2, we describe the sample shape and classify evaluation methods based on the sample shape. In Section 3, we describe the experimental conditions (e.g., sliding speed, contact force, lubricant type, temperature, and materials) used to simulate physiological conditions. In Section 4, we discuss future issues concerning the evaluation methods. Finally, in Section 5, we summarize this review.

2 Sample shapes

An overview of studies conducted on the vascular biotribology of medical devices, biomodels, and blood vessels is given in Tables 1, 2, and 3. In many of these studies, the evaluation targets were both the biomodels and the medical devices.

The evaluation methods strongly depend on the sample shape. They are thus divided here into those based on samples with simple and complex shapes, respectively. In the experiments on samples with simple shapes (Table 1), one or both surfaces were flat. In the experiments on samples with complex shapes (Table 3), shapes similar to those of actual medical devices and the actual vasculature system (a tube in a tube) were used. Studies that performed experiments using

Table 1 Summary of studies that performed experiments on samples with simple shapes

Year	Authors	Sample material	Sample shape	Measurement technique and conditions	Coefficient of friction (CoF)
1983	Triolo and Andrade [17]	Oxidized and unoxidized silicone rubber (SR), polyethylene, and fluorinated ethylene propylene.	Two flat surfaces. Apparent surface contact area was 2.7 cm ² .	Sliding speed: 2.5 mm/s. In distilled water, isotonic saline, and blood plasma environment.	None (pulling force was measured).
1990	Nagaoka and Akashi [16]	Catheter with or without hydrophilic polymer surface, which was cut to a length of 5 cm and fixed on a glass plate, vs. crosslinked 100- μ m-thick collagen film.		Inclined plane apparatus. In physiological saline solution. Weight: 100 g.	Molecular weight of 400,000 or more is essential for low surface friction (below 0.035). CoF of uncoated polyurethane (PU) catheter was 0.32.
1990, 1991	Uyama et al. [78,102]	Polymer film obtained via photoinduced graft polymerization vs. glass plate.		Slider that allowed travel at rate of 10 mm/min. In water.	CoF were drastically reduced to less than 0.05 or 0.1 by graft polymerization.
1993	Ikeuchi et al. [69]	Grafted PU vs. alumina ceramic.	Ring on disk.	Thrust-collar apparatus. In distilled water. 0 to 30 mm/s. Contact pressure: 1.3, 13 kPa.	About 0.04.
1996	Nurdin et al. [67]	PU and poly(vinyl pyrrolidone) (PVP)-coated PU catheter vs. Si ₃ N ₄ triangular tip.		Scanning force microscopy (SFM). Samples were scanned under water and phosphate-buffered saline (PBS) solution and applied normal force was increased and decreased periodically.	Tribometric measurements along 500-nm scan line quantified CoF to be 0.05 for coated catheter and 0.50 for native PU catheter.
2004	Ohta et al. [33]	Poly(vinyl alcohol) hydrogel (PVA-H) or SR (box or tubular) vs. chrome.		Friction tester. Dry and wet.	CoF for wet and dry PVA-H was 0.1 and 0.2, respectively. CoF for SR was larger than 0.4.
2008	Ruiz et al. [19]	Surface-modified polypropylene vs. chrome-plated copper.	Plate (10 mm in diameter) on plate.	Rheometer. Normal load: 5 N. Angular velocity: 0.05 rad/s. pH 7.4 buffer was placed on surface.	Grafting notably decreased CoF from 0.28 to 0.05.
2013	Stoimenov et al. [101]	PVA-H vs. metallic and non-metallic biomaterial.	Ball on disk.	Ball (10 mm in diameter) on disk tribometer. Lubricant: deionized (DI) water. Dead weight: 0.52 N. Sliding speed: 0.5–300 mm/s.	Lowest peak CoF was produced by ceramics and glass (CoF < 0.05), followed by metal alloys (CoF < 0.05–0.08). It was highest for polymers (0.4 < CoF < 1.5).
2020, 2021	Lim et al. [9,28]	20-mm-diameter steel plate vs. flat pristine or hydrogel skin-coated polydimethylsiloxane (PDMS) with diameter of 30 mm.		Rheometer (0.1–2 s ⁻¹). Comparison between DI water and surfactant solution. Normal pressure: 10–25 kPa.	CoF of hydrogel skin-coated PDMS with DI water as lubricant ranged from 0.07 to 0.15.
2022	Wang et al. [18]	Coating surface vs. thermoplastic PU surface.	Sample was cut into 4 cm × 4 cm square and adhered to stainless steel slider.	Slider-on-disk method. Total mass of slider and sample was 205 g.	0.06–0.11.

Table 2 Summary of studies that performed experiments on living tissue

Category	Year	Authors	Sample material	Sample shape	Measurement technique and conditions	Coefficient of friction (CoF)
In vivo	1989	Capron and Bruneval [5]	Commercial balloon catheter (2F) vs. rat thoracic aorta.		Blood. Application of balloon catheter in "hard" and "soft" friction regimes in rats.	None ("hard" friction removes whole endothelium and "soft" friction leaves parts intact).
Ex vivo	2002	Caldwell et al. [68]	Phosphonylated low-density polyethylene (LDPE) catheters vs. porcine aorta.	Two cylinders with diameters of 11 mm and lengths of 12 mm vs. flattened aorta.	Reciprocated friction apparatus (25 mm/s, 192 g, porcine serum).	Average maximum CoF of untreated LDPE was 0.0384, significantly greater than that of phosphonylated LDPE (0.0285).
In vitro	2007	Dunn et al. [10]	Polished glass pin (radius: 7.78 mm) vs. single layer of bovine artery endothelial cells.		Reciprocating sliding. Sliding speed: 0.3 mm/s. Average applied load: 0.4 mN.	0.03–0.06.
Ex vivo	2006, 2007	Takashima et al. [55,71]	Steel ball vs. flattened porcine aorta.		Universal tester and indenter assembly. In physiological saline solution.	0.046 (mean dynamic CoF).
Ex vivo	2008	Kazmierska et al. [72]	Commercial catheter vs. flattened porcine aorta or porcine bladder mucosa.		One-direction movement (10 mm/s). In distilled water.	Static CoF: 0.01–0.13. Dynamic CoF: 0.01–0.09 (for aorta).
Ex vivo	2010	Prokopovich et al. [73]	Silicone elastomer or PU vs. aorta or vena cava from lambs.	Flat (10 mm square) on flat.	Sliding velocity: 30 mm/s. Normal load: 4 N. With or without defibrinated horse blood as lubricant.	0.16–1.35 (dry and wet).
Ex vivo	2012	Flaction et al. [75]	Cylinder vs. flattened bovine hearts.		Sliding speed: 0.2, 0.5 mm/s. Blood and saline water.	None (frictional force).
Ex vivo	2013	Prokopovich et al. [74]	Polyvinylchloride (PVC) catheter vs. flattened porcine aorta.		Sliding speed: 30 mm/s. Pressure: 20000 N/m ² . With or without defibrinated horse blood as lubricant.	0.68 (dry), 0.78 (wet).
In vivo	2017	Matsubara et al. [93]	Commercial coil vs. 10 unruptured human intracranial aneurysms.		Manual insertion.	None (maximum insertion force: 1.42 N).
Ex vivo	2020	Lin et al. [22]	PU ball (φ16 mm) with or without PLL (poly-L-lysine) and HA (hyaluronan) coating vs. flattened porcine aorta.		Reciprocating sliding (6 mm/s). In PBS solution at around 37°C. Normal load was 0.6 N.	Clear differences in CoF. For 8-layer PLL-HA coating, CoF remained at 0.02.
Ex vivo	2020	Lin et al. [70]	Catheter loop vs. flattened porcine aorta.		Reciprocating sliding. In PBS at 37°C. Normal load: 0.3–1.2 N. Sliding speed: 2–10 mm/s.	Increasing sliding speed caused increase in CoF. Increase in normal load first caused decrease and then increase in CoF.
Ex vivo	2020	Wan et al. [20]	PU ball (φ16 mm) with or without polyethylene glycol functionalized hyaluronic acid coating vs. flattened porcine aorta.		Reciprocating sliding (6 mm/s). PBS solution at around 37°C. Normal load: 0.6 N.	CoF for PU started very low (~0.03) but increased gradually up to 0.17, significantly higher than that for coated samples.
Ex vivo and simple shapes	2023	Morita et al. [41]	Commercial resin or porcine artery plates vs. alumina ball (φ 15 mm).		Translational friction tester. Air or saline. Normal force: 50 gf. Speed: 1 m/min.	Dynamic CoF of porcine artery in saline was 0.0547. CoF of resin with silicone coating was similar.

Table 3 Summary of studies that performed experiments on samples with complex shapes

Year	Authors	Sample material and shape	Measurement technique and conditions of frictional force
1991	Uyama et al. [78]	Catheter obtained via photoinduced graft polymerization vs. PVC tube.	Pullout force from PVC tube with water.
1996	Marmieri et al. [79]	Polyurethane catheter vs. tube filled with agar.	Time to pulling out.
1997	Ogata et al. [7]	Commercial catheter or guidewire vs. water-filled polyurethane tube (100 cm in length and 2 mm in inner diameter) with three loops (30, 20, and 15 cm in diameter).	Frictional resistance between guidewires and catheters was measured by pushing guidewires in and out with stroke of 40 mm and speed of 500 mm/min.
2010	Nagano et al. [35]	Silicone rubber aneurysm model ($\phi 4$ mm) vs. commercial coil.	Insertion force during continuous insertion by wire delivery device (0.5 to 2.0 mm/s) or manual operation by doctor. Water.
2012	Guo et al. [61]	Catheter vs. commercial silicone rubber blood vessel model (EVE, FAIN-Biomedical Inc.).	Insertion force by robotic catheter system (master-slave). Average operating force was about 1.5 N.
2012	Kobayashi and Sekine [31]	Guidewire vs. PVA-H curved blood vessel model.	Torque transmission and rotational response.
2013	Haraguchi et al. [38]	Silicone rubber aneurysm model ($\phi 5$ mm) vs. commercial coil.	Insertion force during continuous insertion by wire delivery device (1.0 mm/s).
2014	Lamano et al. [40]	Acrylic aneurysm model ($\phi 3$ mm) with latex membrane vs. commercial coil.	Membrane and insertion force by compression strength testing machine. Insertion speed: 0.17 to 0.83 mm/s.
2014, 2017	Takashima et al. [26,27]	Torus-shaped PVA-H blood vessel model vs. commercial guidewire or catheter.	Force applied to blood vessel model during automatic insertion.
2015	Morris et al. [99]	Commercially available coronary stent system vs. three phantom patient-specific thin-walled compliant coronary vessels.	Insertion force during continuous insertion (8 mm/s). Evaluation of pulsatile flow and dynamic cardiac wall conditions.
2020	Haga et al. [25]	PVA-H 3D blood vessel model vs. microcatheter or guidewire.	Local pressure during manual insertion.
2020	Lim et al. [9]	2D serpentine tunnel-shaped blood vessel model (pristine or hydrogel skin-coated) vs. commercial guidewire.	Insertion force during 1–8 mm/s insertion. DI water or surfactant solution.
2021	Forman et al. [82]	Adenowires and three commercial wires with proprietary hydrophilic coating vs. 2D coronary model system (ASTM 2394).	Insertion and withdrawal forces measured using interventional device testing equipment (IDTE, Machine Solutions).
2021	Klink et al. [77]	Plastic tube with inner lumen diameter of 3 mm attached to pegboard vs. commercial guidewire.	Insertion force and vessel (tube) displacement.
2021, 2022	Takashima et al. [36,37]	Silicone rubber or PVA-H aneurysm model ($\phi 5$ mm) vs. commercial coil.	Insertion force during continuous insertion (1 mm/s). Water.
2022	Kwak et al. [39]	PDMS patient-specific vascular model coated with lubricating layer vs. three commercially available stent retriever devices.	Initial and maximum force during withdrawal (1 mm/s). With saline solution. Pulsatile blood pump was used to generate pulsating flow.
2022	Lee et al. [8]	Biomedical-grade polyimide tube (surface modified) vs. urethane tube (inner diameter: 2 mm).	Insertion force using IDTE. Filled with DI water, 15 mm/s.
2022	Liu et al. [50]	Polytetrafluoroethylene (PTFE), FEP, acrylic tube vs. NiTi shaft.	Insertion force evaluated by pulling flexible shaft made from nitinol through pair of grips made from material used for channel (0.06–0.10).
2022	Zhang et al. [97]	Guidewire ($\phi 0.33$ mm) vs. 30°- and 45°-bent tube (5 mm).	Insertion force. 1 mm/s. Physiological saline and simulated blood solution. With or without vibration of wire.
2023	Leroy et al. [83]	Peripherally inserted central venous catheters vs. ASTM 2394 model.	Insertion and retraction force evaluated using IDTE. 100 cm/min. DI water at 37°C.

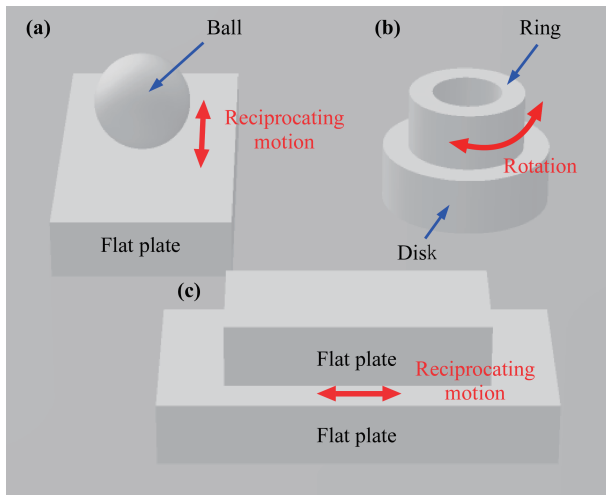


Fig. 2 Examples of simple sample shapes and relative motions. (a) Ball on flat plate (point contact). (b) Ring on disk (area contact). (c) Flat plate on flat plate (area contact).

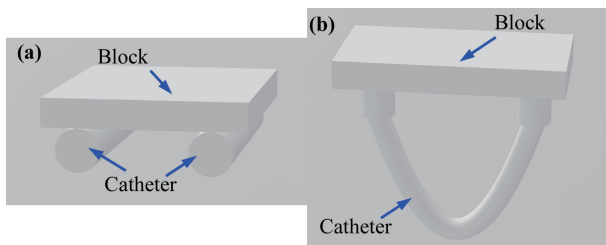


Fig. 3 Examples of simple sample shapes consisting of cylinders and flat surfaces (line contact). (a) Two cylinders fastened to a specimen holder. (b) Catheter loop.

living tissue, regardless of sample shape, are summarized in Table 2.

As shown in Tables 1, 2, and 3, coefficient of friction (CoF) values are used to evaluate the frictional properties for samples with simple shapes, and other parameters, such as insertion force and traction force, are used to evaluate those for samples with complex shapes.

2.1 Simple shapes

Examples of simple sample shapes (Table 1) are shown in Figs. 2 and 3. Samples with these shapes, rather than the tubular complex shape of medical devices, are adopted because they can be easily modified and characterized. For example, samples with simple shapes can be evaluated using standard tribological tests, allowing the use of commercial friction testers and rheometers [9, 19, 28, 33]. Simple shapes are suitable for testing the material itself. The calculated CoF values can be utilized to compare experimental results from different studies. Moreover, it is useful to characterize a given sample using both atomic force microscopy [67, 68] and a friction test even though the trends of nano- and macroscale friction can differ [68].

As shown in Figs. 2 and 3, various sample shapes can be used to measure the frictional force. As shown in Figs. 2 and 3, the contact geometry can be classified into point, line, or area contact. The contact geometry affects the contact mechanism (e.g., lubricating film formation). Unlike for line and area contact, uneven contact is not a concern for point contact;

however, the contact area may change during the experiment due to wear. In addition, it is easier to prepare a flat plate than a ball. For reciprocating motion, the effect of static friction during changes in motion direction should be considered. For the thrust-collar apparatus (Fig. 2(b)), since the nominal contact area has a ring configuration between concentric circles, no leading or trailing edge exists, so internal friction owing to viscoelastic deformation is excluded from the measurements [69]. When selecting a contact geometry, it is important to carefully consider the optimal contact geometry for the purpose of the test.

A combination of a cylinder and a flat surface (Fig. 3) can be used to model a device because most intravascular devices are flexible cylinders. Caldwell et al. [68] used two low-density polyethylene cylinders fastened to a specimen holder, which produced a line contact geometry when articulated against the intima of the aorta by a reciprocating friction apparatus (Fig. 3(a)). For this combination, commercial medical devices can be used. For example, Lin et al. [70] rubbed a porcine aorta (adopted to mimic a human blood vessel) with a catheter loop in reciprocating sliding mode to examine the role of catheter loop curvature, stiffness, normal load, sliding speed, and the endothelial glycocalyx layer on the friction properties (Fig. 3(b)). Nagaoka and Akashi [16] fixed a 5-cm-long catheter on a glass plate and evaluated it using an inclined plane apparatus where one end of the plate was gradually inclined to obtain the initial angle required for slipping to start.

Various types of relative motion, such as linear reciprocation and rotation, can be applied to samples with simple shapes. Most types of apparatus use motors. An inclined plane apparatus [16, 55, 71] that uses gravity can also be used.

However, most experimental models fail to account for the initial deformation of the vessel wall before and after contact because the specimens are in contact with each other at the outset of the experiment and already deformed by an applied load. That is, these models consider the continuation of the contact state, not the initial contact. Takashima et al. [55, 71] investigated the frictional interaction between a blood vessel and a catheter using an apparatus in which a steel ball approached and slid against an inclined and flattened porcine aorta, which deformed gradually as the ball approached.

It is useful to compare CoF values obtained for biomodels with those of blood vessels (Table 2) [10, 20, 22, 41, 55, 68, 70–74]. In many cases, cut and flattened animal aorta, which are commonly used, have CoF values in the range of 0.01–0.13 [41, 55, 68, 71, 72]. When untreated polymers were used, the same samples were repeatedly used, or the blood vessel surface was degraded (note that such conditions do not represent clinical practice), larger CoF values were obtained [20, 22, 70]. Furthermore, Prokopovich et al. [73, 74] reported relatively large CoF values (0.16–0.78) obtained with defibrinated horse blood as a lubricant and assumed that these large CoF values can be attributed to the difference between the commonly used water and blood as the lubricant. The difference in sample shape which contacts the blood vessel could have also contributed to the large values (Prokopovich et al. evaluated the contact interactions of aorta against a flat polymer surface, although a ball or cylinder was used in many studies, as shown in Table 2).

2.2 Complex shapes

Experiments that more closely replicate an actual situation require samples with complex shapes (Table 3). As shown in Table 3, parameters such as insertion force and traction force

(not CoF) are used to evaluate the frictional properties for the samples with complex shapes. The combination of two tubes (a tube in a tube) requires the bending of the outer tube to realize contact. Therefore, to evaluate the frictional properties of the guidewire itself, the wire is often drawn through a circular loop of a polyethylene catheter (internal diameter: 1.57 mm) [76]. In many cases, a tube was fixed in a curved shape and a commercial guidewire was inserted. For example, Klink et al. [77] used plastic tubing attached to a pegboard prepared with graph paper as a background; the pegboard structure and the course of the curves were based on common standards and guidelines [13]. Liu et al. [50] used two tubes and acrylic constraints as a hollow channel. Uyama et al. [78] used polyvinylchloride tube. Marmieri et al. [79] used a tube filled with agar and evaluated the slipperiness of the catheter surfaces using a pull-out test, where the catheter was pulled out from the tube. It was reported that the difference between various combinations became more obvious when guidewires were pushed in rather than pulled out, suggesting that the rigidity of the guidewires was a significant factor [7].

Experiments using more complex vascular models made of silicone rubber [29, 35–39], acrylic [40], poly(vinyl alcohol) hydrogel [25–27, 30–33], and elastomer-hydrogel skin multilayers [9, 28] that mimic living tissue have also been conducted. 3D printers are widely used to prepare biomodels and can easily fabricate mold copies of the vascular tree, which is subsequently embedded in a liquid resin that solidifies into a solid biomodel. After the liquid resin has solidified, the mold material is removed using the lost-wax technique [29]. The increasing availability of 3D printers has led to an increase in the use of complex vascular models. Complex biomodels can realistically simulate a situation where the medical device slides inside a tortuous human blood vessel. Complex patient-specific biomodels are thus useful for testing medical devices prior to their use in humans. A public database of human brain arterial vasculature obtained using magnetic resonance angiography can be used to prepare such models [80].

Several companies (e.g., Instron, Zwick Roell, and Machine Solutions, Inc.) produce test machines for analyzing the behavior of a guidewire and/or catheter [8, 81–83]. For example, testing was performed at Machine Solutions, Inc. using an interventional device testing equipment system to track a catheter through a test fixture constructed according to the American Society for Testing and Materials (ASTM) standard F 2394–07 [13, 81–83].

As shown in Table 3, most studies measured the insertion force of the medical device. Note that the insertion force is the sum of forces applied to all vessel parts by long flexible

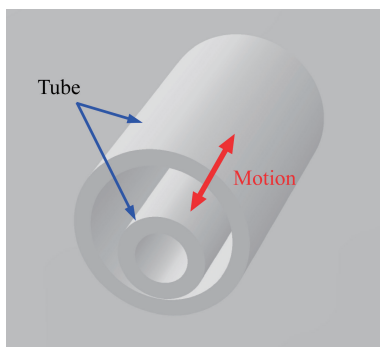


Fig. 4 Model of tube in tube

medical devices. Moreover, the insertion force includes the friction among the medical devices (e.g., the friction between the catheter and the guidewire). For example, a previous study found a difference between the coil insertion force and the contact force of a coil on the aneurysmal dome using an aneurysm model [40]. In order to measure local properties (e.g., contact pressure), it is necessary to use a model tube equipped with small sensors [25, 30]. Catheter-type tactile sensors, which measure force based on the piezoresistance effect [84–86], capacitance [84], optical measurement [87, 88], pressure-sensitive rubber response [89], or piezoelectric effect [90–92], can be used to measure the contact force.

The measured insertion force should be compared with that measured for insertion into the human body. However, there is little *in vivo* data [5, 93], as shown in Table 2. Matsubara et al. [93] measured the coil insertion force for cases of intracranial aneurysm (10 unruptured human intracranial aneurysms) using a force sensor that they had developed.

In tests that use samples with complex shapes, in addition to the insertion force, trackability and pushability are often used as evaluation criteria because friction affects the motion of the medical devices. Trackability refers to the ability of a system to be advanced to the target lesion; it is affected by factors such as friction and bending stiffness [66]. For a model that uses a tube inside a tube, the outside tube must be transparent to allow the positions of the medical devices to be measured [32, 33]. Pushability characterizes the load transfer from the proximal (interventionist's) end to the distal tip of the catheter. High load transfer allows finer and more direct tactile control of the instrumentation [66]. Pushability and trackability are important characteristics of endovascular therapy devices, although there are trade-offs with respect to design, material selection, manufacturing, and tolerance [66]. Because twisting motion is applied to a guidewire to change tip direction, the torque transmission and rotational response of the guidewire in a curved blood vessel are important [31]. The frictional properties along both the axial and circumferential directions of the blood vessel model should thus be discussed.

The frictional properties between a model with a complex shape and a medical device can be initially tested by touch to determine the slipperiness of a sample. With this subjective approach, all samples must be tested at the same time. Therefore, many researchers have evaluated not only the target samples but also standard samples under standardized conditions.

Samples with complex shapes have the following problems.

- The number and positions of the contact points vary with time during insertion, making it difficult to understand the effect at each contact point. The frictional force depends on the changing contact force and area. Moreover, because it is difficult to keep the contact conditions constant, it is also difficult to conduct repeated tests to evaluate wear.
- It is necessary to cut the vessel model into small pieces in order to characterize the surface properties.
- The insertion force into the blood vessel model, not the CoF, is measured. Therefore, another experiment is necessary to measure the CoF. For example, Liu et al. [50] measured the CoF by pulling a flexible shaft made from nitinol through a pair of grips made from the material used for the curved channel.
- Fabrication repeatability is low. It is difficult to repeatedly prepare the same shape accurately. Moreover, it is difficult to measure the shape of the inner surface.

3 Experimental conditions

In order to evaluate the samples shown in Section 2, experiments that simulate physiological conditions should be conducted. Friction includes not only surface force interactions such as interfacial adhesion, asperities deformation, and viscous film shear, but also morphological reaction forces due to surface viscoelastic deformation under the front of the slider [75]. In any case, it is necessary to adopt clinical situations that often occur or that cause problems (e.g., injure living tissues). Note that the non-clinical performance testing recommended for a device's intended use may vary based on its risk profile associated with the intended target vasculature (e.g., coronary, peripheral, and neurovascular) [94]. The conditions that should be considered are described below.

3.1 Sliding speed

It is well known that sliding speed strongly affects the mode of lubrication and the CoF. Therefore, the insertion speed of a medical device may affect the evaluation results; however, a database of actual insertion speeds is not currently available. As shown in Tables 1, 2, and 3, in many studies, the sliding speed (controlled by electric motors) was several millimeters per second. One reason for the speed selection could have been that the speed was consistent with the subjective judgment of the surgeon. However, in the near future, useful information will be obtained from prior research where the speed derived from the tracking data of a catheter or guidewire was proposed as a metric for evaluating surgical skill [95, 96].

3.2 Contact force

Fliation et al. [75] reported that the applied normal force is the dominant factor that affects the frictional force, as determined through experiments that use a cylindrical tip and bovine hearts. They also reported that when a normal force is applied, the areas of contact between the cylinder and the tissue play an important role [75]. The frictional resistance between the guidewire and a vascular wall is also affected by the contact time [97]. A negative correlation between the CoF and normal load is commonly observed for soft tissue, such as skin, intestines, and the esophagus [70].

Although the effect of the contact force is large, similar to the sliding speed described in Section 3.1, a database of contact force is not currently available. One reason for this is that although many catheter-type tactile sensors [84–92] have been proposed, there are no established and approved methods for measuring the contact force in vivo. Moreover, it is difficult to measure the actual normal force between a flexible intravascular device and tortuous blood vessels because the contact state (e.g., number of contact points and reaction force from the medical devices) greatly changes depending on the conditions, such as vascular structure (which varies among individuals), the clearance between the device and the vessel, and the mechanical properties (e.g., stiffness of the medical device). For example, a higher device stiffness leads to higher bending and normal contact force and friction [76]. As various devices with different stiffnesses are used according to the required pushability [66], flexibility, and kink resistance [7], it is difficult to measure the actual normal force under all practical conditions.

In many experiments on samples with simple shapes (see Section 2.1), a weight was used to change the contact force. For in vivo experiments, the inflation amount of a balloon catheter can be used to control the contact conditions [5].

3.3 Lubricant

Water and saline solution were used as the lubricant in many studies. Test conditions such as the soak time are particularly important for hygroscopic materials, whose properties may change with exposure to water or other fluids [13]. Therefore, some samples should be hydrated with aqueous solution prior to testing [19, 28, 83]. When blood is used, heparin can be added to avoid coagulation [75]. Note that the lubricating effect of plasma [17] can reduce the frictional force.

The CoF of an elastomer is higher than that of a blood vessel. Therefore, when an elastomer biomodel is applied in the evaluation of medical devices, medical education, surgical training, or surgical planning, a surfactant solution (e.g., 300 μ M Tween 20 in deionized water) can be used as a lubricant to better mimic a human blood vessel [9]. However, the use of a surfactant solution may cause various problems, such as microbubble generation [9].

3.4 Temperature

Ideally, the test path should be maintained at 37°C to simulate physiological conditions. This is important for the mechanical properties of hydrophilic or hydrophobic coatings of catheters, which are associated with low-friction gliding, and for the mechanics of polymer devices [66]. Several experimental systems have been maintained at physiological conditions (lubricant at 37°C) for the duration of the test sequence [20, 83]. However, because temperature control systems are bulky and expensive, many experiments are conducted at room temperature. For example, Kazmierska et al. [72] and Prokopovich et al. [73] performed all measurements at room temperature because it has been reported [100] that the CoF between rabbit's visceral pleura and parietal pleura is not affected by temperature in the range of 19–39°C for a sliding velocity of up to 30 mm/s. According to the temperature dependence of the test materials and the lubricant, the temperature should be maintained at 37°C or room temperature.

3.5 Materials

Common materials used for vascular biomodel applications include polyurethane, polyamide (Nylon), polytetrafluoroethylene (PTFE), steel, TiNi, and TiMoSn [101]. Most catheters are coated with a lubricious film, such as hydrophilic poly(vinyl pyrrolidone), poly(2-methacryloyloxyethyl phosphorylcholine-co-n-butyl methacrylate) ([poly(MPC-co-BMA)], or ComfortCoat® [70]. The effect of hydrophilicity is large and thus the surface properties of the models are often investigated in terms of the contact angle using liquid droplets [9, 102]. Note that polyethylene has a tendency to acquire memory of the loops of tubing in which the catheter was tested over time [7]. Guidewire stiffness varies with length (for example, flexible 50-mm tip, moderate 50-mm stent/balloon support, and stiff 500-mm shaft); guidewire materials may have a strong nonlinear response and recovery from bending [13]. It may be necessary to simulate the lesion material (e.g., calcium, fibrin, collagen, fat, cholesterol, endothelial cells, smooth muscle cells, red blood cells, platelets, dead white blood cells, and macrophages), type, and morphology [13].

When lubricious coatings are incorporated to decrease the frictional force, coating integrity testing should be conducted because coating separation (e.g., peeling, flaking, shedding delamination, and/or sloughing off) or degradation may adversely impact clinical performance [94].

3.6 Other parameters

Other physiological parameters must also be considered. For example:

- The material properties (e.g., stiffness) of samples can affect the stress concentration at the contact surface. The stiffness of not only the vessel itself but also the surrounding tissue (e.g., muscle and fat) can affect the results [25, 71]. A vascular model created with a soft material similar to an artery may require surrounding materials, such as a gel [103]. Moreover, the constraint force of a vessel (e.g., radial and longitudinal tension) and tangential forces affect the shearing force between the contact points.
- The surface roughness can affect the experimental results. For example, the increased roughness of a phosphonylated low-density polyethylene sample may help trap fluid in the valleys, producing fluid film lubrication, as suggested by the microelastohydrodynamic model, under appropriate operating conditions [68].
- It has been reported that continuous insertion at a constant speed into silicone that simulates an aneurysm requires half or less of the maximum force required for intermittent insertion by a doctor, presumably because static friction is exerted when the insertion is paused [35].
- A pulsatile blood pump has been used to generate a pulsating flow with approximately physiological conditions [39]. Khoshbakht et al. [98] showed that fluid flow can greatly change the tip contact force when the catheter is close to the left inferior pulmonary vein. Moreover, Morris et al. [99] showed that cardiac motion with pulsatile flow significantly changes the insertion forces of a commercially available coronary stent system inserted into three patient-specific coronary artery models.

After non-clinical performance tests, clinical studies are needed to demonstrate how the reduced insertion and retraction forces measured under simulated use conditions translate to ease of insertion scores and clinical outcomes (e.g., reduced potential for vessel wall injury) [83]. Additional clinical trials are needed to determine whether the differences in frictional properties between several devices translate into improved clinical outcomes (e.g., reductions in vascular injury, catheter failure, and rate of infection) [83].

4 Future issues

As shown above, it is difficult to compare the experimental results obtained using different evaluation methods. Therefore, it is necessary to establish standardized methods for evaluating the friction between an intravascular device and a vascular biomodel. There are currently no standardized models of the coronary vasculature, peripheral vasculature, and neurovasculature. Nevertheless, an example of a tracking fixture previously accepted by the United States Food and Drug Administration in premarket submissions is described in Figure X2.4 of ASTM F2394-07 [13, 94]. Although this model simulates a coronary vessel in a 2-D plane, 3D biomodels are useful for realistically simulating an actual situation where the medical device slides inside a tortuous human blood vessel. A public database of human arterial vasculature can be used to prepare a standard artery model [80]. For comparisons of human arterial vasculature, which varies among individuals, it is also necessary to calculate the appropriate parameters to express the blood vessel structures (e.g., curvature and torsion [3]). To keep conditions constant, standard medical devices are necessary

for the evaluation of blood vessel models, and vice versa. As described in Section 2.1, experiments that use samples with simple shapes have many advantages; standardized methods using such samples are also necessary. The combination of several standardized tests using samples with simple and complex shapes would also be useful. As described in Section 3, a database of experimental conditions (e.g., insertion speed and contact force) is not currently available. Clinical data should thus be collected and compiled.

5 Conclusion

In this review, we summarized methods for evaluating the friction between an intravascular medical device and a vascular biomodel. We presented the current state of research on the vascular biotribology of medical devices, biomodels, and blood vessels. We described the sample shape, classified the evaluation methods based on the sample shape, and described each method. Moreover, we described the experimental conditions used to simulate physiological conditions. Finally, we discussed the future issues concerning the evaluation methods. It is necessary to establish standardized methods for evaluating the friction between an intravascular device and a vascular biomodel that can realistically simulate an actual situation where the medical device slides inside a tortuous human blood vessel.

Acknowledgements

This work was partially supported by the Policy Research Project on Regulatory Science of Pharmaceuticals and Medical Devices (Ministry of Health, Labour and Welfare of Japan, 2023). The authors thank FORTE Science Communications (<https://www.forte-science.co.jp/>) for English language editing.

References

- [1] Hillen B. The variability of the circle of Willis: Univariate and bivariate analysis. *Acta Morphol Neerl Scand.* 1986;24: 87–101.
- [2] Schafer S, Hoffmann KR, Noël PB, Ionita CN, Dmochowski J. Evaluation of guidewire path reproducibility. *Med Phys.* 2008;35: 1884–1892. <https://doi.org/10.1118/1.2903430>
- [3] Hoshina M, Oshima M, Torii R. Parametric study of three-dimensional morphology of the cerebral arterial circle of Willis. *Seisan-Kenkyu.* 2005;57: 48–52. <https://doi.org/10.11188/seisankenkyu.57.48>
- [4] Lauric A, Safain MG, Hippelheuser J, Malek AM. High curvature of the internal carotid artery is associated with the presence of intracranial aneurysms. *J Neurointerv Surg.* 2014;6: 733–739. <https://doi.org/10.1136/neurintsurg-2013-010987>
- [5] Capron L, Bruneval P. Influence of applied stress on mitotic response of arteries to injury with a balloon catheter: Quantitative study in rat thoracic aorta. *Cardiovasc Res.* 1989;23: 941–948. <https://doi.org/10.1093/CVR/23.11.941>
- [6] Wagner RMF, Maiti R, Carré MJ, Perrault CM, Evans PC, Lewis R. Bio-tribology of vascular devices: A review of tissue/device friction research. *Biotribology.* 2021;25: 100169. <https://doi.org/10.1016/J.BIOTRI.2021.100169>
- [7] Ogata N, Goto K, Uda K. An evaluation of the physical properties of current microcatheters and guidewires. The development of the “catheter-glide approach” in response to weaknesses of current materials. *Interv Neuroradiol.* 1997;3: 65–80.

- <https://doi.org/10.1177/159101999700300107>
- [8] Lee DU, Kim DW, Lee SY, Choi DY, Choi SY, Moon KS, et al. Amino acid-mediated negatively charged surface improve antifouling and tribological characteristics for medical applications. *Colloids Surfaces B Biointerfaces*. 2022;211: 112314. <https://doi.org/10.1016/j.colsurfb.2021.112314>
- [9] Lim J, Kim J. 3D vascular replicas composed of elastomer-hydrogel skin multilayers for simulation of endovascular intervention. *Adv Funct Mater*. 2020;30: 2003395. <https://doi.org/10.1002/ADFM.202003395>
- [10] Dunn AC, Zaveri TD, Keselowsky BG, Sawyer WG. Macroscopic friction coefficient measurements on living endothelial cells. *Tribol Lett*. 2007;27: 233–238. <https://doi.org/10.1007/S11249-007-9230-0>
- [11] Vad S, Eskinazi A, Corbett T, McGloughlin T, Vande Geest JP. Determination of coefficient of friction for self-expanding stent-grafts. *J Biomech Eng*. 2010;132: 121007. <https://doi.org/10.1115/1.4002798>
- [12] Roy D, Kauffmann C, Delorme S, Lerouge S, Cloutier G, Soulez G. A literature review of the numerical analysis of abdominal aortic aneurysms treated with endovascular stent grafts. *Comput Math Methods Med*. 2012;2012: 1–16. <https://doi.org/10.1155/2012/820389>
- [13] F2394 standard guide for measuring securement of balloon expandable vascular stent mounted on delivery system. 2017. <https://www.astm.org/f2394-07r17.html> (accessed September 26, 2023)
- [14] Nelson J, Patel D, Sant HJ, Shea J, Gale BK, Agarwal J. Compression of the vascular wall to create a friction fit in a vascular anastomotic coupler. *J Mech Behav Biomed Mater*. 2021;123: 104681. <https://doi.org/10.1016/j.jmbm.2021.104681>
- [15] Brewster R, Gale BK, Sant HJ, Monson K, Shea J, Agarwal J. A biodegradable vascular coupling device for end-to-end anastomosis. *J Med Biol Eng*. 2018;38: 715–723. <https://doi.org/10.1007/s40846-017-0348-8>
- [16] Nagaoka S, Akashi R. Low-friction hydrophilic surface for medical devices. *Biomaterials*. 1990;11: 419–424. [https://doi.org/10.1016/0142-9612\(90\)90098-B](https://doi.org/10.1016/0142-9612(90)90098-B)
- [17] Triolo PM, Andrade JD. Surface modification and characterization of some commonly used catheter materials. II. Friction characterization. *J Biomed Mater Res*. 1983;17: 149–165. <https://doi.org/10.1002/JBM.820170112>
- [18] Wang X, Wang J, Yu Y, Yu L, Wang Y, Ren K, et al. A polyzwitterion-based antifouling and flexible bilayer hydrogel coating. *Compos Part B Eng*. 2022;244: 110164. <https://doi.org/10.1016/j.compositesb.2022.110164>
- [19] Ruiz JC, Alvarez-Lorenzo C, Taboada P, Burillo G, Bucio E, De Prijk K, et al. Polypropylene grafted with smart polymers (PNIPAAm/PAAc) for loading and controlled release of vancomycin. *Eur J Pharm Biopharm*. 2008;70: 467–477. <https://doi.org/10.1016/j.ejpb.2008.05.020>
- [20] Wan H, Lin C, Kaper HJ, Sharma PK. A polyethylene glycol functionalized hyaluronic acid coating for cardiovascular catheter lubrication. *Mater Des*. 2020;196: 109080. <https://doi.org/10.1016/j.matdes.2020.109080>
- [21] Lanigan JL, Fatima S, Charpentier TV, Neville A, Dowson D, Bryant M. Lubricious ionic polymer brush functionalised silicone elastomer surfaces. *Biotribology*. 2018;16: 1–9. <https://doi.org/10.1016/j.biotri.2018.08.001>
- [22] Lin C, Wan H, Kaper HJ, Sharma PK. A hyaluronic acid based lubricious coating for cardiovascular catheters. *Tribol Int*. 2020;151: 106495. <https://doi.org/10.1016/j.triboint.2020.106495>
- [23] Roth Y, Lewitus DY. The grafting of multifunctional antithrombogenic chemical networks on polyurethane intravascular catheters. *Polym*. 2020;12: 1131. <https://doi.org/10.3390/POLYM12051131>
- [24] Mitsudou K. PTCA technique. Igaku Shoin. 1999.
- [25] Haga Y, Yoshida H, Matsunaga T, Shimizu Y, Ohta M, Shojima M, et al. Cerebrovascular model equipped with microsensors. *IEEE Trans Sensors Micromachines*. 2020;140: 354–362. <https://doi.org/10.1541/ieejsmas.140.354>
- [26] Takashima K, Oike A, Yoshinaka K, Yu K, Ohta M, Mori K, et al. Evaluation of the effect of catheter on the guidewire motion in a blood vessel model by physical and numerical simulations. *J Biomech Sci Eng*. 2017;12: 17-00181-17–00181. <https://doi.org/10.1299/jbse.17-00181>
- [27] Takashima K, Tsuzuki S, Ooike A, Yoshinaka K, Yu K, Ohta M, et al. Numerical analysis and experimental observation of guidewire motion in a blood vessel model. *Med Eng Phys*. 2014;36: 1672–1683. <https://doi.org/10.1016/j.medengphy.2014.09.012>
- [28] Lim J, Hwang J, Kim J. Rapid and accurate manufacture of 3D vascular replicas with smooth inner surfaces using wax-coated molds. *Adv Mater Technol*. 2021;6: 2100220. <https://doi.org/10.1002/ADMT.202100220>
- [29] Wetzel SG, Ohta M, Handa A, Auer JM, Lylyk P, Lovblad KO, et al. From patient to model: Stereolithographic modeling of the cerebral vasculature based on rotational angiography. *AJNR Am J Neuroradiol*. 2005;26: 1425–1427.
- [30] Moriwaki T, Okamoto Y, Yamaga H, Fujisaki K, Uematsu M, Sakoda H, et al. In vitro measurement of contact pressure applied to a model vessel wall during balloon dilation by using a film-type sensor. *J Neuroendovascular Ther*. 2022;16: 192–197. <https://doi.org/10.5797/jnet.0a.2021-0068>
- [31] Kobayashi S, Sekine K. Torque transmission and rotational response characteristics of medical guide-wire in curved blood vessel model. *J Fiber Bioeng Informatics*. 2012;5: 273–279. <https://doi.org/10.3993/jfbi09201205>
- [32] Yu C, Kosukegawa H, Mamada K, Kuroki K, Takashima K, Yoshinaka K, et al. Development of an in vitro tracking system with poly (vinyl alcohol) hydrogel for catheter motion. *J Biomech Sci Eng*. 2010;5: 11–17. <https://doi.org/10.1299/jbse.5.11>
- [33] Ohta M, Handa A, Iwata H, Rüfenacht DA, Tsutsumi S. Polyvinyl alcohol hydrogel vascular models for in vitro aneurysm simulations: The key to low friction surfaces. *Technol Heal Care*. 2004;12: 225–233. <https://doi.org/10.3233/thc-2004-12302>
- [34] Shimizu Y, Tupin S, Kiyomitsu C, Kitamura K, Takashima K, Ohta M. Development of a stereo dip-coating system for fabrication of tube-shaped blood vessel models. *Sci Reports*. 2020;10: 6929. <https://doi.org/10.1038/s41598-020-63718-w>
- [35] Nagano Y, Nishio Y, Matsubara N, Miyachi S, Fujimoto H. Surgical support system for cerebral aneurysm coil embolization. *NTN Tech Rev*. 2010;78: 122–128.
- [36] Takashima K, Ikeda Y, Yoshinaka K, Ohta M, Mori K, Toma N. Evaluation of contact force between aneurysm model and coil for embolization of intracranial aneurysms. *J Neuroendovascular Ther*. 2021;15: 233–239. <https://doi.org/10.5797/JNET.OA.2020-0069>
- [37] Oishi T, Takashima K, Yoshinaka K, Yu K, Ohta M, Mori K, et al. Evaluation of effect of aneurysm model material on coil contact force and catheter movement. *J Biomech Sci Eng*. 2022;17: 21–00261. <https://doi.org/10.1299/JBSE.21-00261>

- [38] Haraguchi K, Miyachi S, Matsubara N, Nagano Y, Yamada H, Marui N, et al. A mechanical coil insertion system for endovascular coil embolization of intracranial aneurysms. *Interv Neuroradiol.* 2013;19: 159–166.
<https://doi.org/10.1177/159101991301900203>
- [39] Kwak Y, Son W, Kim BJ, Kim M, Yoon SY, Park J, et al. Frictional force analysis of stent retriever devices using a realistic vascular model: Pilot study. *Front Neurol.* 2022;13: 1902.
<https://doi.org/10.3389/FNEUR.2022.964354>
- [40] Lamano JB, Bushnell GG, Chen H, Badrinathan A, El Tecle NE, Bendok BR, et al. Force characterization of intracranial endovascular embolization. *Neurosurgery.* 2014;75: 707–716.
<https://doi.org/10.1227/NEU.0000000000000525>
- [41] Morita R, Nonoyama T, Abo D, Soyama T, Fujima N, Imai T, et al. Mechanical properties of a 3 dimensional-printed transparent flexible resin used for vascular model simulation compared with those of porcine arteries. *J Vasc Interv Radiol.* 2023;34: 871–878.
<https://doi.org/10.1016/J.JVIR.2023.01.008>
- [42] Alderliesten T, Konings MK, Niessen WJ. Modeling friction, intrinsic curvature, and rotation of guide wires for simulation of minimally invasive vascular interventions. *IEEE Trans Biomed Eng.* 2007;54: 29–38.
<https://doi.org/10.1109/TBME.2006.886659>
- [43] Roszelle BN, Nair P, Gonzalez LF, Haithem Babiker M, Ryan J, Frakes D. Comparison among different high porosity stent configurations: Hemodynamic effects of treatment in a large cerebral aneurysm. *J Biomech Eng.* 2014;136: 021013.
<https://doi.org/10.1115/1.4026257>
- [44] Nejati-Aghdam A, Tavallaei MA. Modeling and prediction of a guidewire's reachable workspace and deliverable forces. *IEEE Open J Eng Med Biol.* 2022;3: 227–234.
<https://doi.org/10.1109/OJEMB.2022.3233778>
- [45] Qiao A, Zhang Z. Numerical simulation of vertebral artery stenosis treated with different stents. *J Biomech Eng.* 2014;136: 041007.
<https://doi.org/10.1115/1.4026229>
- [46] Guo J, Guo S, Xiao N, Gao B. Virtual reality simulators based on a novel robotic catheter operating system for training in minimally invasive surgery. *J Robot Mechatronics.* 2012;24: 649–655.
<https://doi.org/10.20965/jrm.2012.p0649>
- [47] Trivisonne R, Kerrien E, Cotin S. Constrained stochastic state estimation of deformable 1D objects: Application to single-view 3D reconstruction of catheters with radio-opaque markers. *Comput Med Imaging Graph.* 2020;81: 101702.
<https://doi.org/10.1016/j.compmedimag.2020.101702>
- [48] Wang Y, Chui C, Lim H, Cai Y, Mak K. Real-time interactive simulator for percutaneous coronary revascularization procedures. *Comput Aided Surg.* 1998;3: 211–227.
<https://doi.org/10.3109/10929089809149843>
- [49] Takashima K, Namba A, Ota H, Haga Y, Ohta M, Mori K, et al. Numerical simulation to evaluate guidewire and catheter behavior during catheter introduction. *J Biomech Sci Eng.* 2023;18: 22–00276.
<https://doi.org/10.1299/JBSE.22-00276>
- [50] Liu J, Cao L, Miyasaka M, Phee SJ. A frictional contact-pattern-based model for inserting a flexible shaft into curved channels. *IEEE/ASME Trans Mechatronics.* 2022;27: 2556–2567.
<https://doi.org/10.1109/TMECH.2021.3111701>
- [51] Sharei H, Alderliesten T, van den Dobbelsteen JJ, Dankelman J. Navigation of guidewires and catheters in the body during intervention procedures: A review of computer-based models. *J Med Imaging.* 2018;5: 1.
<https://doi.org/10.1117/1.JMI.5.1.010902>
- [52] Hong JK, Gao L, Singh J, Goh T, Ruhoff AM, Neto C, et al. Evaluating medical device and material thrombosis under flow: Current and emerging technologies. *Biomater Sci.* 2020;8: 5824–5845.
<https://doi.org/10.1039/D0BM01284J>
- [53] Otani T, Ii S, Shigematsu T, Fujinaka T, Hirata M, Ozaki T, et al. Computational model of coil placement in cerebral aneurysm with using realistic coil properties. *J Biomech Sci Eng.* 2015;10: 15-00555.
<https://doi.org/10.1299/jbse.15-00555>
- [54] Ma D, Dargush GF, Natarajan SK, Levy EI, Siddiqui AH, Meng H. Computer modeling of deployment and mechanical expansion of neurovascular flow diverter in patient-specific intracranial aneurysms. *J Biomech.* 2012;45: 2256–2263.
<https://doi.org/10.1016/j.jbiomech.2012.06.013>
- [55] Takashima K, Shimomura R, Kitou T, Terada H, Yoshinaka K, Ikeuchi K. Contact and friction between catheter and blood vessel. *Tribol Int.* 2007;40: 319–328.
<https://doi.org/10.1016/j.triboint.2005.10.010>
- [56] Xu Y, Mangla S, Gschneidner P, Shi Y. A multi-asperity adhesive contact model for catheter and vascular artery contact in endovascular surgery. *Biomed Microdevices.* 2023;25: 7.
<https://doi.org/10.1007/S10544-023-00646-2>
- [57] Beaman CB, Kaneko N, Meyers PM, Tateshima S. A review of robotic interventional neuroradiology. *Am J Neuroradiol.* 2021;42: 808–814.
<https://doi.org/10.3174/ajnr.A6976>
- [58] Pereira VM, Cancelliere NM, Nicholson P, Radovanovic I, Drake KE, Sungur JM, et al. First-in-human, robotic-assisted neuroendovascular intervention. *J Neurointerv Surg.* 2020;12: 338–340.
<https://doi.org/10.1136/neurintsurg-2019-015671.rep>
- [59] Miyachi S, Nagano Y, Hironaka T, Kawaguchi R, Ohshima T, Matsuo N, et al. Novel operation support robot with sensory-motor feedback system for neuroendovascular intervention. *World Neurosurg.* 2019;127: e617–e623.
<https://doi.org/10.1016/j.wneu.2019.03.221>
- [60] Che Zakaria NA, Komeda T, Low CY, Makoto M, Kobayashi M, Ismail AY, et al. Development of foolproof catheter guide system based on mechatronic design. *Prod Eng.* 2013;7: 81–90.
<https://doi.org/10.1007/S11740-012-0430-6>
- [61] Guo J, Guo S, Xiao N, Ma X, Yoshida S, Tamiya T, et al. A novel robotic catheter system with force and visual feedback for vascular interventional surgery. *Int J Mechatronics Autom.* 2012;2: 15.
<https://doi.org/10.1504/IJMA.2012.046583>
- [62] Zhang L, Guo S, Yu H, Song Y, Tamiya T, Hirata H, et al. Design and performance evaluation of collision protection-based safety operation for a haptic robot-assisted catheter operating system. *Biomed Microdevices.* 2018;20: 22.
<https://doi.org/10.1007/S10544-018-0266-8>
- [63] Negoro M, Tanimoto M, Arai F, Fukuda T, Fukasaku K, Takahashi I, et al. An intelligent catheter system robotic controlled catheter system. *Interv Neuroradiol.* 2001;7: 111–113.
<https://doi.org/10.1177/15910199010070S116>
- [64] Martel S, Mathieu JB, Felfoul O, Chanu A, Aboussouan E, Tamaz S, et al. Automatic navigation of an untethered device in the artery of a living animal using a conventional clinical magnetic resonance imaging system. *Appl Phys Lett.* 2007;90: 114105.
<https://doi.org/10.1063/1.2713229>
- [65] Tognarelli S, Castelli V, Ciuti G, Di Natali C, Sinibaldi E, Dario P, et al. Magnetic propulsion and ultrasound tracking of endovascular devices. *J Robot Surg.* 2012;6: 5–12.
<https://doi.org/10.1007/s11701-011-0332-1>
- [66] Lanzer P, ed. *Mastering endovascular techniques: A guide to excellence.* Lippincott Williams & Wilkins. 2007.
- [67] Nurdin N, Weilandt E, Textor M, Taborelli M, Spencer ND,

- Descouts P. Reduced frictional resistance of polyurethane catheter by means of a surface coating procedure. *J Appl Polym Sci*. 1996;61: 1939–1948.
[https://doi.org/10.1002/\(SICI\)1097-4628\(19960912\)61:11<1939::AID-APP8>3.0.CO;2-K](https://doi.org/10.1002/(SICI)1097-4628(19960912)61:11<1939::AID-APP8>3.0.CO;2-K)
- [68] Caldwell RA, Woodell JE, Ho SP, Shalaby SW, Boland T, Langan EM, et al. *In vitro* evaluation of phosphonylated low-density polyethylene for vascular applications. *J Biomed Mater Res*. 2002;62: 514–524.
<https://doi.org/10.1002/JBM.10249>
- [69] Ikeuchi K, Takii T, Norikane H, Tomita N, Ohsumi T, Uyama Y, et al. Water lubrication of polyurethane grafted with dimethylacrylamide for medical use. *Wear*. 1993;161: 179–185.
[https://doi.org/10.1016/0043-1648\(93\)90467-Z](https://doi.org/10.1016/0043-1648(93)90467-Z)
- [70] Lin C, Kaper HJ, Li W, Splinter R, Sharma PK. Role of endothelial glycocalyx in sliding friction at the catheter-blood vessel interface. *Sci Reports*. 2020;10: 11855.
<https://doi.org/10.1038/s41598-020-68870-x>
- [71] Takashima K. Development of tactile sensor and surgical simulator for minimally invasive surgery. Ph. D. Thesis., Kyoto University, Kyoto. 2006.
- [72] Kazmierska K, Szwasz M, Ciach T. Determination of urethral catheter surface lubricity. *J Mater Sci Mater Med*. 2008;19: 2301–2306.
<https://doi.org/10.1007/S10856-007-3339-4>
- [73] Prokopovich P, Perni S, Piccirillo C, Pratten J, Parkin IP, Wilson M. Frictional properties of light-activated antimicrobial polymers in blood vessels. *J Mater Sci Mater Med*. 2010;21: 815–821.
<https://doi.org/10.1007/s10856-009-3882-2>
- [74] Prokopovich P, Perni S. Contact interactions of aorta against PVC catheters. *Tribol Int*. 2013;66: 157–164.
<https://doi.org/10.1016/j.triboint.2013.03.009>
- [75] Flaction L, Hakim B, Rognini G, Verin V, Bleuler H. Screening of the factors influencing frictional interactions between a cylindrical tip and the cardiac wall using factorial analysis. *Tribol Int*. 2012;48: 63–72.
<https://doi.org/10.1016/j.triboint.2011.11.005>
- [76] Schröder J. The mechanical properties of guidewires: Part III: Sliding friction. *Cardiovasc Intervent Radiol*. 1993;16: 93–97.
<https://doi.org/10.1007/BF02602986>
- [77] Klink F, Boese A, Voß S, Beyer C. Design and implementation of a medical device test stand for micro-catheters and guide-wires. *Curr Dir Biomed Eng*. 2021;7: 339–342.
<https://doi.org/10.1515/CDBME-2021-2086>
- [78] Uyama Y, Tadokoro H, Ikada Y. Low-frictional catheter materials by photo-induced graft polymerization. *Biomaterials*. 1991;12: 71–75.
[https://doi.org/10.1016/0142-9612\(91\)90135-W](https://doi.org/10.1016/0142-9612(91)90135-W)
- [79] Marmieri G, Pettenati M, Cassinelli C, Morra M. Evaluation of slipperiness of catheter surfaces. *J Biomed Mater Res*. 1996;33: 29–33.
[https://doi.org/10.1002/\(SICI\)1097-4636\(199621\)33:1<29::AID-JBM5>3.0.CO;2-O](https://doi.org/10.1002/(SICI)1097-4636(199621)33:1<29::AID-JBM5>3.0.CO;2-O)
- [80] Wright SN, Kochunov P, Mut F, Bergamino M, Brown KM, Mazziotta JC, et al. Digital reconstruction and morphometric analysis of human brain arterial vasculature from magnetic resonance angiography. *Neuroimage*. 2013;82: 170–181.
<https://doi.org/10.1016/j.neuroimage.2013.05.089>
- [81] Ramli HR, Arof MAM, Saripan MI, Bello F. Design of a modular testing platform for the handling and study of endovascular devices. 2018 IEEE-EMBS Conf. Biomed. Eng. Sci. 2018: 255–258.
<https://doi.org/10.1109/IECBES.2018.8626628>
- [82] Forman MB, Brewer EC, Brown ZR, Menshikova EV, Lowman AM, Jackson EK. Novel guidewire design and coating for continuous delivery of adenosine during interventional procedures. *J Am Heart Assoc*. 2021;10: e019275.
<https://doi.org/10.1161/JAHA.120.019275>
- [83] LeRoy KJ, Donahue DT. Trackability of a high-strength thromboresistant hydrogel catheter: An *in vitro* analysis comparing venous catheter forces in a simulated use pathway. *J Mech Behav Biomed Mater*. 2023;139: 105670.
<https://doi.org/10.1016/j.jmbbm.2023.105670>
- [84] Eltaib MEH, Hewitt JR. Tactile sensing technology for minimal access surgery—A review. *Mechatronics*. 2003;13: 1163–1177.
[https://doi.org/10.1016/S0957-4158\(03\)00048-5](https://doi.org/10.1016/S0957-4158(03)00048-5)
- [85] Tanimoto M, Arai F, Fukuda T, Iwata H, Itoigawa K, Gotoh Y, et al. Micro force sensor for intravascular neurosurgery and *in vivo* experiment. *Proc. MEMS 98. IEEE. Elev. Annu. Int. Work. Micro Electro Mech. Syst. An Investig. Micro Struct. Sensors, Actuators, Mach. Syst. (Cat. No.98CH36176)*. 1998: 504–509.
<https://doi.org/10.1109/MEMSYS.1998.659809>
- [86] Takizawa H, Tosaka H, Ohta R, Kaneko S, Ueda Y. Development of a microfine active bending catheter equipped with MIF tactile sensors. *Proc IEEE Micro Electro Mech Syst (Cat. No.99CH36291)*. 1999: 412–417.
<https://doi.org/10.1109/MEMSYS.1999.746864>
- [87] Haga Y, Mineta T, Esashi M. Active catheter, active guide wire and related sensor systems. *Proc. 5th Biannu. World Autom. Congr*. 2002: 291–296.
<https://doi.org/10.1109/WAC.2002.1049455>
- [88] Polygerinos P, Puangmali P, Schaeffter T, Razavi R, Seneviratne LD, Althoefer K. Novel miniature MRI-compatible fiber-optic force sensor for cardiac catheterization procedures. 2010 IEEE Int. Conf. Robot. Autom. 2010: 2598–2603.
<https://doi.org/10.1109/ROBOT.2010.5509416>
- [89] Sekitani T, Zschieschang U, Klauk H, Someya T. Flexible organic transistors and circuits with extreme bending stability. *Nat Mater*. 2010;9: 1015–1022.
<https://doi.org/10.1038/nmat2896>
- [90] Takashima K, Ota K, Yamamoto M, Takenaka M, Horie S, Ishida K. Development of catheter-type tactile sensor composed of polyvinylidene fluoride (PVDF) film. *ROBOMECH J*. 2019;6: 19.
<https://doi.org/10.1186/s40648-019-0147-9>
- [91] WeiXing F, HuanRan W, ShuXiang G, KeJun W, XiuFen Y. Design and experiments of a catheter side wall tactile sensor for minimum invasive surgery. 2007 Int. Conf. Mechatronics Autom. 2007: 1073–1078.
<https://doi.org/10.1109/ICMA.2007.4303697>
- [92] Takashima K, Horie S, Mukai T, Ishida K, Matsushige K. Piezoelectric properties of vinylidene fluoride oligomer for use in medical tactile sensor applications. *Sensors Actuators A: Phys*. 2008;144: 90–96.
<https://doi.org/10.1016/j.sna.2008.01.015>
- [93] Matsubara N, Miyachi S, Izumi T, Yamada H, Marui N, Ota K, et al. Clinical application of insertion force sensor system for coil embolization of intracranial aneurysms. *World Neurosurg*. 2017;105: 857–863.
<https://doi.org/10.1016/j.wneu.2017.06.092>
- [94] FDA. Coronary, Peripheral, and Neurovascular Guidewires - Performance Tests and Recommended Labeling. 2019.
<https://www.fda.gov/regulatory-information/search-fda-guidance-documents/coronary-peripheral-and-neurovascular-guidewires-performance-tests-and-recommended-labeling> (accessed September 26, 2023).
- [95] Mazomenos EB, Chang PL, Rippel RA, Rolls A, Hawkes DJ, Bicknell CD, et al. Catheter manipulation analysis for objective

- performance and technical skills assessment in transcatheter aortic valve implantation. *Int J Comput Assist Radiol Surg.* 2016;11: 1121–1131.
<https://doi.org/10.1007/s11548-016-1391-6>
- [96] Guo J, Li M, Wang Y, Guo S. An image information-based objective assessment method of technical manipulation skills for intravascular interventions. *Sensors.* 2023;23: 4031.
<https://doi.org/10.3390/s23084031>
- [97] Zhang C, Liang S, Cao Y, Sun H, Feng L. Reducing the guidewire friction for endovascular interventional surgery by radial micro-vibration. *IEEE Trans Ultrason Ferroelectr Freq Control.* 2022;69: 1020–1031.
<https://doi.org/10.1109/TUFFC.2022.3142763>
- [98] Khoshbakht R, Kheiri M, Dargahi J, Hooshiar A. Effects of blood flow on the tip contact force of cardiac ablation catheters. 2022 IEEE Int. Symp. Robot. Sensors Environ. 2022: 1–7.
<https://doi.org/10.1109/ROSE56499.2022.9977429>
- [99] Morris L, Fahy P, Stefanov F, Finn R. The effects that cardiac motion has on coronary hemodynamics and catheter trackability forces for the treatment of coronary artery disease: An *in vitro* assessment. *Cardiovasc Eng Technol.* 2015;6: 430–449.
<https://doi.org/10.1007/s13239-015-0241-y>
- [100] D'angelo E, Loring SH, Gioia ME, Pecchiari M, Moscheni C. Friction and lubrication of pleural tissues. *Respir Physiol Neurobiol.* 2004;142: 55–68.
<https://doi.org/10.1016/j.resp.2004.05.006>
- [101] Stoimenov B, Fridrici V, Kapsa P, Kosukegawa H, Ohta M. Bioengineering materials and conditions for obtaining low friction with PVA hydrogels. *Tribol Online.* 2013;8: 140–152.
<https://doi.org/10.2474/TROL.8.140>
- [102] Uyama Y, Tadokoro H, Ikada Y. Surface lubrication of polymer films by photoinduced graft polymerization. *J Appl Polym Sci.* 1990;39: 489–498.
<https://doi.org/10.1002/app.1990.070390301>
- [103] Reddy AS, Liu Y, Cockrum J, Gebrezgiabhier D, Davis E, Zheng Y, et al. Construction of a comprehensive endovascular test bed for research and device development in mechanical thrombectomy in stroke. *J Neurosurg.* 2020;134: 1190–1197.
<https://doi.org/10.3171/2020.1.JNS192732>



This paper is licensed under the Creative Commons Attribution-NonCommercial-NoDerivatives 4.0 International (CC BY-NC-ND 4.0) License. This allows users to copy and distribute the paper, only upon conditions that (i) users do not copy or distribute such paper for commercial purposes, (ii) users do not change, modify or edit such paper in any way, (iii) users give appropriate credit (with a link to the formal publication through the relevant DOI (Digital Object Identifier)) and provide a link to this license, and (iv) users acknowledge and agree that users and their use of such paper are not connected with, or sponsored, endorsed, or granted official status by the Licensor (i.e. Japanese Society of Tribologists). To view this license, go to <https://creativecommons.org/licenses/by-nc-nd/4.0/>. Be noted that the third-party materials in this article are not included in the Creative Commons license, if indicated on the material's credit line. The users must obtain the permission of the copyright holder and use the third-party materials in accordance with the rule specified by the copyright holder.